

Flooding and sinking of an originally skimming body

Frank T. Smith · Kevin Liu 

Received: 2 February 2017 / Accepted: 29 June 2017 / Published online: 2 August 2017
© The Author(s) 2017. This article is an open access publication

Abstract The effects of flooding on an originally skimming body in shallow water are analysed. A two-dimensional flow model is presented which is based on mass flux, momentum, a stream-wise pressure jump across the leading edge of the body and an equi-pressure condition at the trailing edge. Linearised and numerical analyses are performed over a wide range of model parameters; the conditions under which a body is able to either emerge from or sink deeper into water are examined, with particular respect to the body's incident angle, rotation, scaled gravity and buoyancy. The findings here enlarge the existing skimming theory and give a first mathematical account of the complete life cycle of a skimming or sinking body.

Keywords Body · Computation · Flooding · Fluid · Interaction · Mathematical modelling · Sinking · Skimming

1 Introduction

The focus of the present work is the flooding over and complete sinking of a body as it fails to skim (skip) over a shallow layer of water. Alternatively the body may re-emerge or erupt from the layer and continue to skim. The body is assumed to be thin and the typical Reynolds number large. The work is motivated by applications in industry especially concerning the trajectories of ice shards along an aircraft fuselage [1–6]. Other applications include surfboarding and skimming [7–10]. There is also intrinsic interest in the fluid-body interactions active here. It is our pleasure to dedicate the article to the Journal of Engineering Mathematics on its 50th anniversary; one of us (FTS) is honoured to have been an editor for over 30 of those years.

Clearly there are many different length scales and possible parameter ranges. We seek common features. “Flooding” occurs frequently in the natural world (e.g. whales and dolphins, swimming and diving) as well as in fields of industry and engineering. For example, observations and experience suggest that a surfboard is often partially immersed under water during surfing. Even a surfboard at rest while carrying the weight of an adult is typically below water (Fig. 1a), and only with sufficient speed can the board usually surf on the ocean's free surface (Fig. 1b). Stone-skipping by the seaside or lakeside is another popular pastime activity. Depending on the surface conditions

F. T. Smith (✉) · K. Liu
University College London, Gower Street, London WC1E 6BT, UK
e-mail: f.smith@ucl.ac.uk

K. Liu
e-mail: kevin.liu@pmb.oxon.org



Fig. 1 Illustrations of flooding or partial flooding over various types of body. From top left clock-wise: **a** a surfboard carrying the weight of an adult surfer at rest, notice that the board's equilibrium position is below the free surface; **b** a surfboard in motion with its rear section being flooded; **c** a ship sails through rough sea with waves flooding over its deck; **d** a snowmobile skims on a shallow layer of water with its skis partially submerged in water. Note the modelling in **a** and **b** ignores the surfer except for a buoyancy effect. **a** Surfboard at rest. **b** Surfboard in motion. **c** Ship in rough sea. **d** Snowmobile's skis partially submerged in water

a stone can penetrate into waves/tides and experience flooding over its entire body. With regard to industrial applications in addition to the aerodynamics ones, a ship sailing through rough seas typically experiences flooding over the top of its deck, see Fig. 1c. A snowmobile travelling at speed is capable of skimming and skipping on shallow water, with its skis experiencing at least partial flooding as shown in Fig. 1d. Torpedo motion is another application together with related military uses. Needless to say, understanding such interactions between liquid (water), solid body and air has a wide range of applications.

The skimming problem of a thin flat finite body over shallow water is investigated in [1,3] (see also [7]); other closely related shallow water entry problems can be found in [11–16]. They model the physical conditions under which a skimming body obtains sufficient lift to achieve liftoff. One of the model assumptions is that the water's free surface is in contact only with the lower section (the underneath) of the body, while its upper section is in contact with air. The present interest, by contrast, is in circumstances where the body may not attain sufficient lift and may sink wholly or partly into the water. The skimming body loses its forward jet (splash) when such flooding occurs. The present aim is to investigate the effects of flooding over a body in skimming motion, to predict whether sinking or re-emergence takes place and in the former case to predict the time for complete sinking to occur.

In the theoretical background close to our concerns, Bowles and Smith [17] investigate a flow past successive multi-blades. The feature of a stream-wise pressure jump in a localised Euler region is deployed at the leading edge of each blade, and the pressure and streamline profiles of the flows are obtained inside the viscous boundary layer

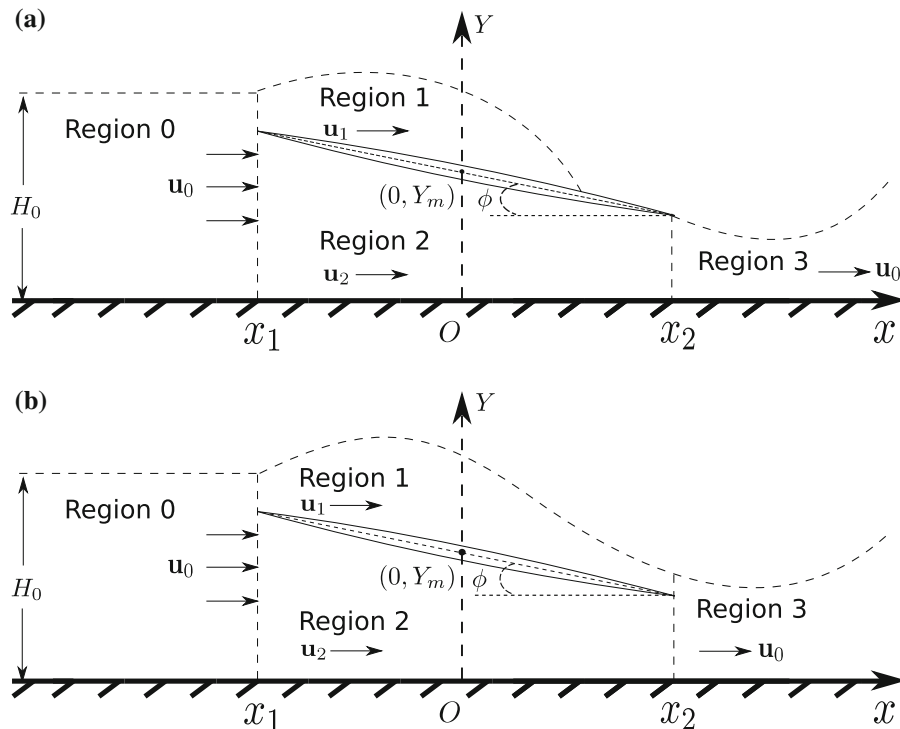


Fig. 2 Sketch of a thin body immersed in shallow water. The body travels leftwards into water at rest. However, the Cartesian coordinate system is introduced such that the x -axis rests at the flow bed pointing rightwards, and the Y -axis points upwards and passes through the body's centre of mass. We shall assume the body has uniform density and is symmetric about its centre of mass. Under this frame of reference the horizontal position of the body's centre of mass is fixed and the fluid flows from left to right in the diagram. **a** Partial flooding over the body. **b** Complete flooding over the body

around the blade as well as in the wake of the flow. Smith and Wilson [18] analyse flow between two solid walls past a blade with a variable thickness and camber, the blade being free to move in the channel and bounce and clash with the solid boundary walls. Kaur [19] studies a flow past a tethered blade. The body of the blade is fixed about a pivot point but is free to rotate so that its angle of attack goes through an unsteady evolution with the flow. The entire blade is again assumed to be immersed in water at all times. Relevant papers including an unknown interface are by [1, 3, 14].

For most moving bodies of interest here, viscosity and surface tension play negligible roles. We also assume the fluid is incompressible and its flow is two-dimensional (2D). The water layer is shallow such that its depth, which is comparable with the body thickness, is much less than the body length. This assumption of shallowness is relevant for various applications. Section 2 describes the detailed model of flooding and sinking. The example of the surfboard is referred to on occasion since it is perhaps most observable; we are aware though of the limitations, e.g. through 3D effects. Sections 3, 4 then present linear and non-linear solution properties, respectively, for the fluid-body interactions involved here while Sect. 5 presents conclusions.

2 The flooding and sinking model

The 2D model consists of a thin body skimming at a small angle on or in a shallow layer of water, with the water flowing both over and below the body. The flow of concern here can be separated into four regions, see Fig. 2. We conduct our analysis in a frame travelling horizontally with the (constant) initial horizontal velocity of the body, such that the horizontal position of the body is fixed for a significant period of time and the water flows from left

to right of the frame, with the body free to move vertically and horizontally as well as rotate about its centre of mass. (The horizontal movement in this frame is found to be negligible over the time scales of present concern, see Sect. 2.3.)

2.1 Scales and interaction structure

Let $\bar{\mathbf{u}} = (\bar{u}, \bar{v})$ denote the flow velocity; except in certain small zones we expect $\bar{u} \gg \bar{v}$ everywhere. In the far upstream and downstream regions the undisturbed flow velocity is given by $\bar{\mathbf{u}}_0 = (\bar{u}_0, 0)$. Supposing the length scale of the body is \bar{L} and the undisturbed water depth is \bar{h}_0 , we non-dimensionalise the model system as

$$x = \frac{\bar{x}}{\bar{L}}, \quad y = \frac{\bar{y}}{\bar{L}}, \quad h = \frac{\bar{h}}{\bar{L}}, \quad t = \frac{\bar{u}_0 \bar{t}}{\bar{L}}, \quad u = \frac{\bar{u}}{\bar{u}_0}, \quad v = \frac{\bar{v}}{\bar{u}_0}, \quad p = \frac{\bar{p}}{\bar{\rho} \bar{u}_0^2}. \quad (1)$$

Here the bar sign is used to denote dimensional variables, with \bar{p} , $\bar{\rho}$ denoting the dimensional pressure and water density, respectively.

The non-dimensionalised Navier–Stokes equations in 2D can be thus written in the following form:

$$\frac{\partial \mathbf{u}}{\partial t} + \mathbf{u} \cdot \nabla \mathbf{u} = -\nabla p - \frac{1}{Fr}(0, 1) + \frac{1}{Re} \nabla^2 \mathbf{u}, \quad (\nabla \cdot \mathbf{u} = 0) \quad (2)$$

with Fr and Re being the Froude and Reynolds numbers, respectively,

$$Fr = \frac{\bar{u}_0^2}{\bar{g} \bar{L}}, \quad Re = \frac{\bar{\rho} \bar{u}_0 \bar{L}}{\bar{\mu}}.$$

In the problems of current interest Re is typically large whereas Fr may be of order unity or large, and so viscous forces are nominally negligible (provided there is no substantial separation [1–3, 18, 20, 21]) whereas gravity effects may not be. Capillary effects are similarly negligible here.

We exploit the large aspect ratio of our model by introducing the following scaling:

$$Y = \frac{y}{\epsilon}, \quad H = \frac{h}{\epsilon}, \quad V = \frac{v}{\epsilon} \quad \left(\epsilon = \frac{\bar{h}_0}{\bar{L}} \ll 1 \right). \quad (3)$$

Assuming the flow is irrotational, the horizontal flow velocity is essentially uniform across the vertical dimension: $u = u(x, t)$. Given that viscous forces are negligible and the ratio ϵ is small, the Navier–Stokes equations (2) reduce to thin-layer equations at the leading order:

$$\frac{\partial u}{\partial t} + u \frac{\partial u}{\partial x} = -\frac{\partial p}{\partial x}, \quad (4a)$$

$$0 = -\frac{\partial p}{\partial Y} - \hat{g}, \quad (4b)$$

where \hat{g} is a scaled gravity term:

$$\hat{g} = \frac{\epsilon}{Fr}. \quad (5)$$

The vertical pressure distribution in our shallow water model is essentially hydrostatic according to (4b).

For the depictions given in Fig. 2 then, the flow from upstream in region 0 has a velocity of $\mathbf{u}_0 = (u_0, 0)$ and flow depth of H_0 . (The horizontal velocity of the body is taken to be supercritical.) This flow is split by the thin

body into two regions: one above the body in region 1; the other below in region 2. We let $\mathbf{u}_1 = (u_1, \epsilon V_1)$ and H_1 denote the flow velocity and depth (measured from the top of the body to the free surface), respectively, in region 1, while the pressure $p_1(x, Y, t)$ is hydrostatic given the shallowness of the water. In region 2 the pressure is denoted as $p_2(x, Y, t)$, and the flow velocity and depth are given as $\mathbf{u}_2 = (u_2, \epsilon V_2)$ and $H_2(x, t)$, respectively. The angle ϕ made between the body and the bed implies the body rotates with scaled angular velocity $\omega = d\phi/dt$. The typical angle of attack in applications is small, usually in the range of $(-20^\circ, 20^\circ)$.

From the water depths of the regions 1 and 2, we can obtain the height of the free-surface elevation $\eta(x, t)$:

$$\eta(x, t) = H_1(x, t) + H_2(x, t). \tag{6}$$

If the upper surface of the body is completely flooded, the flow in region 1 joins the downstream region 3, where the pressure is hydrostatic everywhere and the flow velocity past the body eventually returns to \mathbf{u}_0 as in the original skimming paper [1]. No substantial gravity waves act over these length scales. If on the other hand the board's upper surface is at least partially dry, then there is a gravity-driven wetting process over the dry surface.

Supposing the non-dimensional atmospheric pressure p_0 is zero without losing generality, we integrate the vertical momentum equation (4b) to obtain:

$$p_1(x, Y, t) = \hat{g}(\eta - Y). \tag{7}$$

Hence the pressure in region 1 is hydrostatic. By a similar argument the pressure for region 2 has the form

$$p_2(x, Y, t) = \pi_2(x, t) + \hat{g}(\eta - Y), \tag{8}$$

with π_2 denoting the pressure difference on the lower and upper surfaces of the body:

$$\pi_2(x, t) = p_2(x, H_{2-}, t) - p_1(x, H_{2+}, t). \tag{9}$$

Note that in the case of a body with negligible thickness such that $H_{2-} \sim H_{2+}$, the hydrostatic pressure above and below the body cancels out, and the hydrodynamic pressure π_2 is the only dominant force from the fluid acting on the board. We finally have the pressure conditions (7), (8) in the two regions above and below the board. The flow's horizontal momentum equation (4a) in these two regions can thus be written as

$$\frac{\partial u_1}{\partial t} + u_1 \frac{\partial u_1}{\partial x} = -\hat{g} \frac{\partial \eta}{\partial x}, \tag{10a}$$

$$\frac{\partial u_2}{\partial t} + u_2 \frac{\partial u_2}{\partial x} = -\frac{\partial \pi_2}{\partial x} - \hat{g} \frac{\partial \eta}{\partial x}. \tag{10b}$$

2.2 Boundary and end conditions

As the body moves in the water we assume the flow separates smoothly from its sharp trailing edge into the downstream wake, i.e. a Kutta condition applies here. This is equivalent to imposing the following pressure condition at the trailing edge where $x = x_2$:

$$p_1(x_2, H_2, t) = p_2(x_2, H_2, t) = \hat{g}H_1(x_2, t). \tag{11}$$

What happens at the leading edge is worth a more detailed discussion. First, in a 2D model the flow from upstream splits into two streams, above and below the body, and therefore the mass conservation law dictates that

$$u_0 H_0 = 1 = u_1 H_1 + u_2 H_2, \quad (12)$$

which is the flux condition imposed at the leading edge of the body. (Note that $u_0 = H_0 = 1$ in the non-dimensional variables.) Second, the flow layers above and below the body are different in the sense that if they start with the same pressure conditions they would usually produce different pressure conditions at the trailing edge [17, 18]. This inconsistency with the Kutta condition is resolved by introducing a localised Euler region at the leading edge, where the interactions between the upstream and downstream flows are concentrated; the length scale of this Euler region is $O(\epsilon \bar{L})$ [17]. Therefore on the large horizontal scale what we witness is a flow discontinuity, whereby a pressure jump is present when the flow crosses the leading-edge station into region 1 or 2. Across this discontinuity the stream-wise Bernoulli quantity is conserved from the upstream region through the Euler region around the leading edge, so that

$$p_0 + \frac{1}{2} u_0^2 = p_1 + \frac{1}{2} u_1^2(x_{1+}, t) = p_2 + \frac{1}{2} u_2^2(x_{1+}, t). \quad (13)$$

The comparatively short length scales within the Euler region lead to quasi-steadiness there due to the spatial derivatives being dominant, which yields the jump conditions in (13). Note that unlike the case of a flat body skimming on water, there is no thrown-forward jet at the leading edge in the flooding case. Moreover from (13) the free surface is discontinuous (with a jump) at the leading edge.

Regarding the normal boundary conditions, at the flow bed $Y = 0$ the non-penetrable boundary implies

$$V(x, 0, t) = 0. \quad (14)$$

On the free surface, given the large aspect ratio the leading order kinematic boundary condition in region 2 is

$$V(x, H_2, t) = \frac{\partial H_2}{\partial t} + u_2 \frac{\partial H_2}{\partial x}. \quad (15)$$

Additionally the incompressibility condition for the fluid can be vertically integrated in region 2 to give

$$V(x, H_2, t) = -H_2 \frac{\partial u_2}{\partial x}. \quad (16)$$

Combining the two conditions (15) and (16), we obtain the following (shallow water) conservation equation:

$$\frac{\partial H_2}{\partial t} + \frac{\partial}{\partial x}(u_2 H_2) = 0. \quad (17)$$

Similarly in region 1 we find

$$\frac{\partial H_1}{\partial t} + \frac{\partial}{\partial x}(u_1 H_1) = 0. \quad (18)$$

2.3 The free body movement

Concerning the motion of the body itself, using arguments similar to the flat body skimming case in [1, 3] we have the vertical and angular momentum equations:

$$\int_{x_1}^{x_2} (p_2 - p_1) dx = \int_{x_1}^{x_2} \left[\pi_2(x, t) + \frac{\epsilon}{Fr} T(x) \right] dx = \hat{m} \left(\frac{d^2 y_m}{dt^2} + \frac{1}{Fr} \right), \tag{19a}$$

$$\int_{x_1}^{x_2} (p_2 - p_1) x dx = \int_{x_1}^{x_2} \left[\pi_2(x, t) + \frac{\epsilon}{Fr} T(x) \right] x dx = \hat{i} \frac{d^2 \phi}{dt^2}, \tag{19b}$$

to leading order, since the angles involved are small and as such $\cos \phi \sim 1$. Here $T(x)$ denotes the scaled body thickness; \hat{m} and \hat{i} are the scaled mass and moment of inertia such that $\hat{m} = \bar{m}/\bar{\rho}\bar{L}^2, \hat{i} = \bar{i}/\bar{\rho}\bar{L}^4$; the $\int_{x_1}^{x_2} T(x) dx$ term represents the (scaled) water mass displaced by the solid body. We further take the horizontal positions (x_1, x_2) of the leading and trailing edges as $(-1, 1)$. The momentum equations for the body (19) can be written in the following form:

$$\int_{-1}^1 \pi_2(x, t) dx = M \left[\frac{d^2 Y_m}{dt^2} + \frac{1}{\epsilon Fr} - \frac{1}{M} \frac{\epsilon}{Fr} \int_{-1}^1 T(x) dx \right], \tag{20a}$$

$$\int_{-1}^1 \pi_2(x, t) x dx = I \frac{d^2 \theta}{dt^2} - \frac{\epsilon}{Fr} \int_{-1}^1 x T(x) dx, \tag{20b}$$

with $Y_m = y_m/\epsilon$ and with M, I, θ given as

$$M = \epsilon \hat{m}, \tag{21a}$$

$$I = \epsilon \hat{i}, \tag{21b}$$

$$\phi = \epsilon \theta. \tag{21c}$$

Note that M, I, θ take on order unity values typically.

The term $-\frac{\epsilon}{Fr} \int_{-1}^1 T(x) dx$ in (20a) represents the buoyancy force exerted on the body. Without taking such force into account, a surfboard carrying the weight of a human would sink when not in surfing motion, which is different from reality (see Fig. 1a). The buoyancy effect also can play an important role in numerous industrial and other applications. It is convenient for us to introduce a buoyancy parameter \hat{A} as follows:

$$\hat{A} = \frac{1}{\epsilon Fr} - \frac{1}{M} \frac{\epsilon}{Fr} \int_{-1}^1 T(x) dx. \tag{22}$$

This is the Archimedean gravity force representing the acceleration due to the net effects of buoyancy and gravity. For the case $\hat{A} = 0$, the body’s buoyancy cancels out its gravitational effect; $\hat{A} > 0$ represents the case that gravity overcomes buoyancy and vice versa. We shall further neglect the torque force due to buoyancy in the angular momentum equation (20b)—and assume the body has a uniform density so that any change in angular momentum is purely due to the hydrodynamic effect of the flow. We can now re-write the body momentum equations as

$$\int_{-1}^1 \pi_2(x, t) dx = M \left(\frac{d^2 Y_m}{dt^2} + \hat{A} \right), \tag{23a}$$

$$\int_{-1}^1 x \pi_2(x, t) dx = I \frac{d^2 \theta}{dt^2}. \tag{23b}$$

The horizontal momentum balance in the body motion, on the other hand, is such that the horizontal momentum must remain constant since the horizontal forces are comparatively small [1, 5, 7, 11] (The scaling after (3) indicates that the horizontal pressure force is of order ϵ compared with the vertical one.) Hence the body and the coordinate frame of reference continue to move horizontally with equal uniform speed over the current time scales.

2.4 Summary of fluid-body interaction

To summarise, we have the following governing equations for the flow above the body in region 1:

$$\frac{\partial H_1}{\partial t} + \frac{\partial}{\partial x}(u_1 H_1) = 0, \quad (24a)$$

$$\frac{\partial u_1}{\partial t} + u_1 \frac{\partial u_1}{\partial x} = -\hat{g} \frac{\partial}{\partial x}(H_1 + H_2), \quad (24b)$$

$$p_1(x, Y, t) = \hat{g}(H_1 + H_2 - Y), \quad (24c)$$

$$u_1^2(-1, t) - 2\hat{g}[1 - H_1(-1, t) - H_2(-1, t)] - 1 = 0, \quad (24d)$$

$$p_1(1, H_2, t) = \hat{g}H_1(1, t). \quad (24e)$$

The condition (24e) is equivalent to requiring smooth behaviour at the trailing-edge point, given the relation (24c). Also in region 2 we have

$$\frac{\partial H_2}{\partial t} + \frac{\partial}{\partial x}(u_2 H_2) = 0, \quad (25a)$$

$$\frac{\partial u_2}{\partial t} + u_2 \frac{\partial u_2}{\partial x} = -\frac{\partial \pi_2}{\partial x} - \hat{g} \frac{\partial}{\partial x}(H_1 + H_2), \quad (25b)$$

$$H_2(x, t) = Y_m + x\theta, \quad (25c)$$

$$p_2(x, Y, t) = \pi_2(x, t) + \hat{g}(H_1 + H_2 - Y), \quad (25d)$$

$$\pi_2(-1, t) + \frac{1}{2}[u_2^2(-1, t) - 1] + \hat{g}[H_1(-1, t) + H_2(-1, t) - 1] = 0, \quad (25e)$$

$$u_1(-1, t)H_1(-1, t) + u_2(-1, t)H_2(-1, t) = 1, \quad (25f)$$

$$p_2(1, H_2, t) = \hat{g}H_1(1, t). \quad (25g)$$

Finally for the solid body we have the following governing equations:

$$\int_{-1}^1 \pi_2(x, t) dx = M \left(\frac{d^2 Y_m}{dt^2} + \hat{A} \right), \quad (26a)$$

$$\int_{-1}^1 x \pi_2(x, t) dx = I \frac{d^2 \theta}{dt^2}. \quad (26b)$$

We have therefore developed a complete flooding model, as shown in Fig. 2b, for a thin body that is originally in planing motion. The initial conditions are covered case by case below. The scenario shown in Fig. 2a of partial flooding is also covered by allowance for changes in the conditions within any dry part. This flooding model (24)–(26) consists of six unknowns u_1 , u_2 , H_1 , Y_m , θ and π_2 , with \hat{g} , \hat{A} being static parameters (assumed to be constant forces) prescribed according to the specific physical context. For the remainder of this study we analyse this flooding model via both analytical and numerical treatments.

3 Linearised analysis of the flooding interaction

The integro-differential system (24)–(26) is difficult to analyse in its current form. Any solution will need to be pursued numerically. Before we pursue such solutions, it is possible to gain some insights by working with a linearised version of this flooding system. We introduce a small amplitude parameter δ such that $\delta \ll 1$, and asymptotically expand the system variables in the following manner:

$$\hat{g} = \delta \bar{g}, \tag{27a}$$

$$\hat{A} = \delta \bar{A}, \tag{27b}$$

$$Y_m = 1 + \delta Y_1(t), \tag{27c}$$

$$\theta = 1 + \delta \theta_1(t), \tag{27d}$$

$$H_1 = 0 + \delta H_{11}(x, t), \tag{27e}$$

$$H_2 = 1 + \delta H_{21}(x, t), \tag{27f}$$

$$u_1 = 1 + \delta u_{11}(x, t), \tag{27g}$$

$$u_2 = 1 + \delta u_{21}(x, t), \tag{27h}$$

$$p_1 = 0, \tag{27i}$$

$$p_2 = 0 + \delta \pi_{21}(x, t). \tag{27j}$$

The basic state here has uniform horizontal velocities of unity in regions 1, 2 for a body which is thin relative to the thickness of the liquid layer, and the flow depth above the body is shallow ($\sim O(\delta)$) compared with the depth below ($\sim O(1)$). Note that to limit the complexity of our linearised system, the gravity and buoyancy effects in our flow model are restricted to be small ($\sim O(\delta)$).

3.1 Linearised system

Substituting these expansions into the system (24)–(26), we obtain the following relations for the flow in region 1:

$$\frac{\partial H_{11}}{\partial t} + \frac{\partial H_{11}}{\partial x} = 0, \tag{28a}$$

$$\frac{\partial u_{11}}{\partial t} + \frac{\partial u_{11}}{\partial x} = 0, \tag{28b}$$

$$u_{11}(-1, t) = 0. \tag{28c}$$

Likewise in region 2 we have the following relations after the asymptotic expansions:

$$\frac{\partial H_{21}}{\partial t} + \frac{\partial H_{21}}{\partial x} + \frac{\partial u_{21}}{\partial x} = 0, \tag{29a}$$

$$\frac{\partial u_{21}}{\partial t} + \frac{\partial u_{21}}{\partial x} + \frac{\partial \pi_{21}}{\partial x} = 0, \tag{29b}$$

$$\pi_{21}(-1, t) + u_{21}(-1, t) = 0, \tag{29c}$$

$$H_{21} = Y_1 + x\theta_1. \tag{29d}$$

The flux conditions at the leading edge and the Kutta condition at the trailing edge can be written as follows:

$$H_{11}(-1, t) + H_{21}(-1, t) + u_{21}(-1, t) = 0, \tag{30a}$$

$$\pi_{21}(1, t) = 0. \tag{30b}$$

The momentum equations of the immersed body become

$$M \left(\frac{\partial^2 Y_1}{\partial t^2} + \bar{A} \right) = \int_{-1}^1 \pi_{21} dx, \quad (31a)$$

$$I \frac{\partial^2 \theta_1}{\partial t^2} = \int_{-1}^1 x \pi_{21} dx. \quad (31b)$$

The flow velocity and depth in (28a) and (28b) can be solved analytically, their solutions being arbitrary functions of the composite variable $x - t$:

$$H_{11} = \mathfrak{h}(x - t), \quad (32a)$$

$$u_{11} = \mathfrak{u}(x - t). \quad (32b)$$

Provided that the initial and leading-edge boundary conditions for H_{11} and u_{11} are known, their solutions can be fully traced out along the straight characteristics $x - t = c$. For our current analysis we suppose there is no flooding over the top of the body initially, that is to say

$$H_{11}(x, 0) = 0, \quad (33a)$$

$$u_{11}(x, 0) = 0. \quad (33b)$$

The initial condition (33a) for the flow velocity u_{11} together with its boundary condition (28c) implies that it has the following trivial solution:

$$u_{11}(x, t) = 0, \quad (34)$$

and therefore the flooding over the top of the body occurs at the same speed as the undisturbed upstream velocity, i.e. $u_1 = u_0 = 1$.

In region 2, the flow velocity u_{21} can be solved by substituting (29d) into (29a) and directly integrating with respect to x :

$$u_{21} = -\frac{x^2}{2} \frac{d\theta_1}{dt} - x \frac{dY_1}{dt} - x\theta_1 - \mathcal{U}(t), \quad (35)$$

where $\mathcal{U}(t)$ is an unknown function of time as a result of the spatial integration. Substituting this solution into (29b) and integrating with respect to x we obtain the following solution for π_{21} :

$$\pi_{21} = \frac{x^3}{6} \frac{d^2\theta_1}{dt^2} + \frac{x^2}{2} \frac{d^2Y_1}{dt^2} + x^2 \frac{d\theta_1}{dt} + x \frac{d\mathcal{U}}{dt} + x \frac{dY_1}{dt} + x\theta_1 + \mathcal{P}(t), \quad (36)$$

where $\mathcal{P}(t)$ is an unknown function of time resulting again from spatial integration. From the solutions of the flow velocity u_{21} and the dynamic pressure π_{21} in region 2, we find the following relation based on the linearised Bernoulli principle at the leading edge (29c):

$$\frac{1}{2} \frac{d^2Y_1}{dt^2} - \frac{1}{6} \frac{d^2\theta_1}{dt^2} + \frac{1}{2} \frac{d\theta_1}{dt} - \frac{d\mathcal{U}}{dt} + \mathcal{P} - \mathcal{U} = 0. \quad (37)$$

Similarly the flux condition at the leading edge (30a) implies

$$\mathfrak{h}(-1 - t) + \frac{dY_1}{dt} - \frac{1}{2} \frac{d\theta_1}{dt} + Y_1 - \mathcal{U} = 0. \quad (38)$$

The Kutta condition at the trailing edge (30b) together with the pressure equation (36) then gives

$$\frac{1}{6} \frac{d^2\theta_1}{dt^2} + \frac{1}{2} \frac{d^2Y_1}{dt^2} + \frac{d\theta}{dt} + \frac{dY_1}{dt} + \frac{dU}{dt} + \theta_1 + \mathcal{P} = 0. \tag{39}$$

The immersed body’s momentum equations can be now written as

$$\left(M - \frac{1}{3}\right) \frac{d^2Y_1}{dt^2} - \frac{2}{3} \frac{d\theta_1}{dt} - 2\mathcal{P} + M\bar{\mathcal{A}} = 0, \tag{40a}$$

$$\left(3I - \frac{1}{5}\right) \frac{d^2\theta_1}{dt^2} - 2\frac{dY_1}{dt} - 2\frac{dU}{dt} - 2\theta_1 = 0. \tag{40b}$$

We have finally rearranged the linearised flooding model into a system of five equations (37)–(40) with five unknowns $Y_1, \theta_1, \mathfrak{h}(-1 - t), U$ and \mathcal{P} . These five equations can be further simplified to the following form:

$$(\mathcal{K} + 1) \frac{d^2Y_1}{dt^2} = -\frac{5}{6} \frac{d\theta_1}{dt} - \frac{dY_1}{dt} - \theta_1 + U - M\bar{\mathcal{A}}, \tag{41a}$$

$$\left(\mathcal{L} + \frac{1}{3}\right) \frac{d^2\theta_1}{dt^2} = -\frac{1}{2} \frac{d\theta_1}{dt} + \frac{dY_1}{dt} + \theta_1 - U, \tag{41b}$$

$$(6\mathcal{L} + 2) \frac{dU}{dt} = -(3\mathcal{L} + 2) \frac{dY_1}{dt} - \frac{3\mathcal{L}}{2} \frac{d\theta_1}{dt} - (3\mathcal{L} + 2)\theta_1 - 3\mathcal{L}U, \tag{41c}$$

for Y_1, θ_1, U where \mathcal{K} and \mathcal{L} are constants given by

$$\mathcal{K} = M - \frac{1}{3}, \tag{42a}$$

$$\mathcal{L} = 3I - \frac{1}{5}. \tag{42b}$$

3.2 Solution properties

Equations (41a) to (41c) can be written as a system of linear equations

$$\begin{bmatrix} \dot{Y}_1 \\ \dot{\theta}_1 \\ \dot{U} \\ \dot{V}_1 \\ \dot{\omega}_1 \end{bmatrix} = \begin{bmatrix} 0 & 0 & 0 & 1 & 0 \\ 0 & 0 & 0 & 0 & 1 \\ 0 & -\frac{3\mathcal{L}+2}{6\mathcal{L}+2} & -\frac{3\mathcal{L}}{6\mathcal{L}+2} & -\frac{3\mathcal{L}+2}{6\mathcal{L}+2} & -\frac{3\mathcal{L}}{12\mathcal{L}+4} \\ 0 & -\frac{1}{\mathcal{K}+1} & \frac{1}{\mathcal{K}+1} & -\frac{1}{\mathcal{K}+1} & -\frac{5}{6(\mathcal{K}+1)} \\ 0 & \frac{3}{3\mathcal{L}+1} & -\frac{3}{3\mathcal{L}+1} & \frac{3}{3\mathcal{L}+1} & -\frac{3}{6\mathcal{L}+2} \end{bmatrix} \begin{bmatrix} Y_1 \\ \theta_1 \\ U \\ V_1 \\ \omega_1 \end{bmatrix} - \begin{bmatrix} 0 \\ 0 \\ 0 \\ \frac{M\bar{\mathcal{A}}}{\mathcal{K}+1} \\ 0 \end{bmatrix}, \tag{43}$$

where V_1 and ω_1 are defined, respectively, as

$$V_1 = \frac{dY_1}{dt}, \tag{44a}$$

$$\omega_1 = \frac{d\theta_1}{dt}. \tag{44b}$$

We solved the system (41) via a finite-difference scheme with the following initial conditions: $\bar{\mathcal{A}} = 1, Y_1(0) = 0, \theta_1(0) = 0, V_1(0) = -1, \omega_1(0) = 0, \mathfrak{h}(-1) = 0$ and $U(0) = Y_1(0) + V_1(0) - 0.5\omega_1(0)$, with $M = 1$ and $I = \frac{1}{4}$.

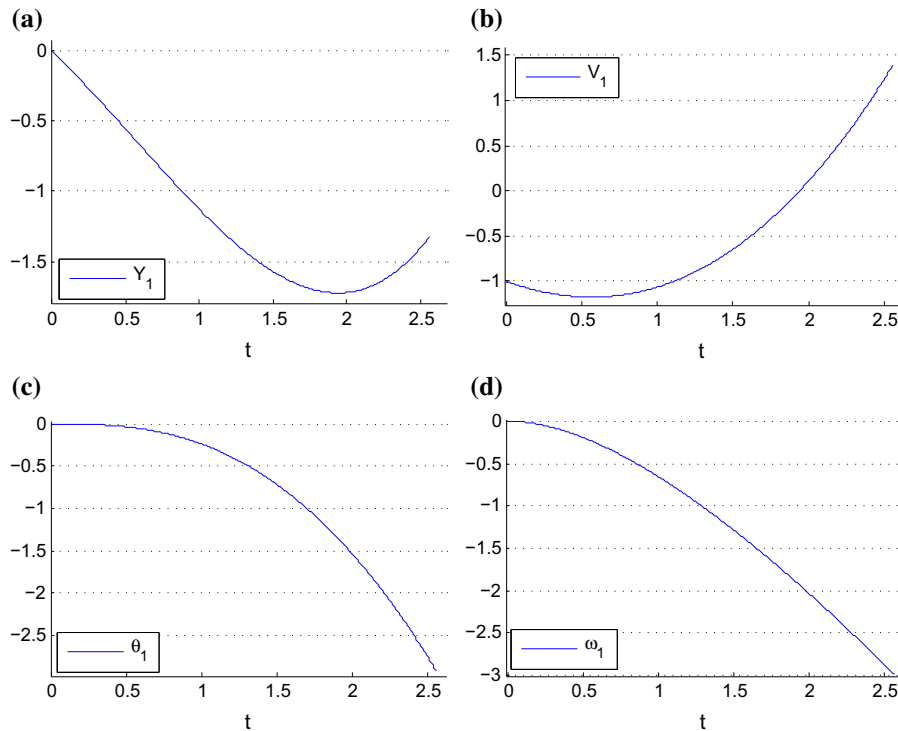


Fig. 3 The linearised vertical and angular motions of a thin body becoming flooded over time. This system is configured with initial conditions of $\theta_1(0) = 0$, $\omega_1(0) = 0$ and scaled vertical velocity of $V_1(0) = -1$. The scaled gravity for the body is set to $\bar{A} = 1$. **a** Y_1 . **b** V_1 . **c** θ_1 . **d** ω_1

Under such configurations, the body is able to obtain sufficient lift to ascend in water, which is signified by the slope of the vertical velocity V_1 of the body turning positive at $t \sim 0.6$, as shown in Fig. 3b. The linear system (43) configured with such initial conditions has the following five eigenvalues: $(0, 0, 0.269, -0.873 \pm 0.284i)$. The existence of a positive eigenvalue indicates that our solutions grow exponentially with time: the body's vertical position continues to rise and its contact angle becomes more acute until the solutions grow beyond the linearised regime. We ensure, however, that h_1 is never negative.

Figure 4 shows the solutions for the water depth above the body. Figure 4a shows the depth of flooding over the leading edge of the body, while Fig. 4b demonstrates the water depth over the entire body at various times. We terminate the solution at around $t \sim 2.56$, at which point the body is in vertical ascendancy while the water depth above its leading edge is decreased to zero. From that time onwards the body is in a skimming process without flooding as analysed in [1, 3]. Figure 5 gives the corresponding evolution of velocity and pressure under the body.

Once the board's initial velocities ($V_1(0)$, $\omega_1(0)$) and vertical position $Y_1(0)$ are known, Eq. (38) shows that $\mathfrak{h}(-1)$ can be configured to match the incoming flood depth at the leading edge by setting an appropriate value of $\mathcal{U}(0)$, which in turn also has an effect on the velocity of the flow underneath the body and thus on the lift.

Figure 6 shows the effect of the gravity parameter \bar{A} (or g) on our linearised flooding model. The greater the gravity effect, the deeper this body sinks into water before reversing its course. From a modelling perspective, a greater \bar{A} corresponds to a body with less buoyancy in the water.

4 Non-linear flooding: numerical solutions

In this section, we introduce a numerical scheme for solving the flooding system of (24)–(26). The solutions to the flow in region 1 and 2 are coupled with each other via the flux condition at the leading edge and Kutta condition at

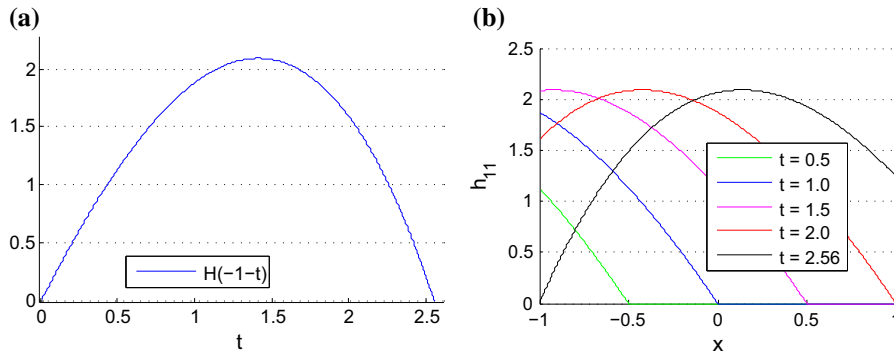


Fig. 4 **a** Shows $h(-1-t)$, i.e. the depth of the water above the plate at the leading edge. At $t \sim 2.56$, the depth becomes negative, which signifies the leading edge of the body emerges from water and the flooding process terminates. **b** Shows the water depth profile at various times. **a** $h(-1-t)$. **b** H_{11}

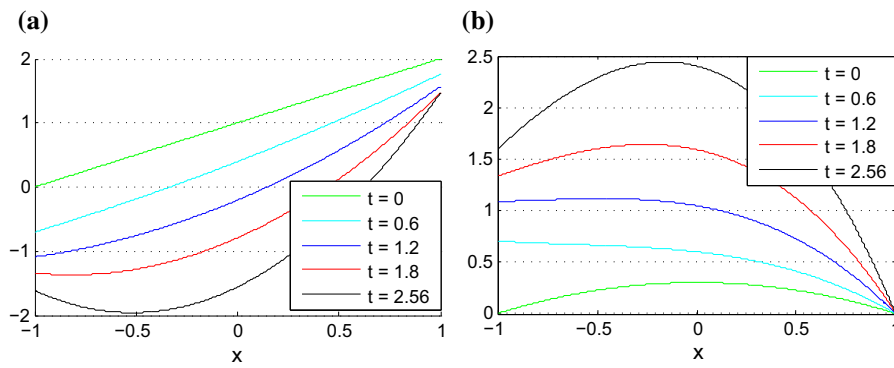


Fig. 5 Solutions of the flow velocity and pressure underneath the body at various times. The flow velocity becomes negative in a region including the leading edge, which corresponds to a positive pressure in such region. **a** u_{21} . **b** π_{21}

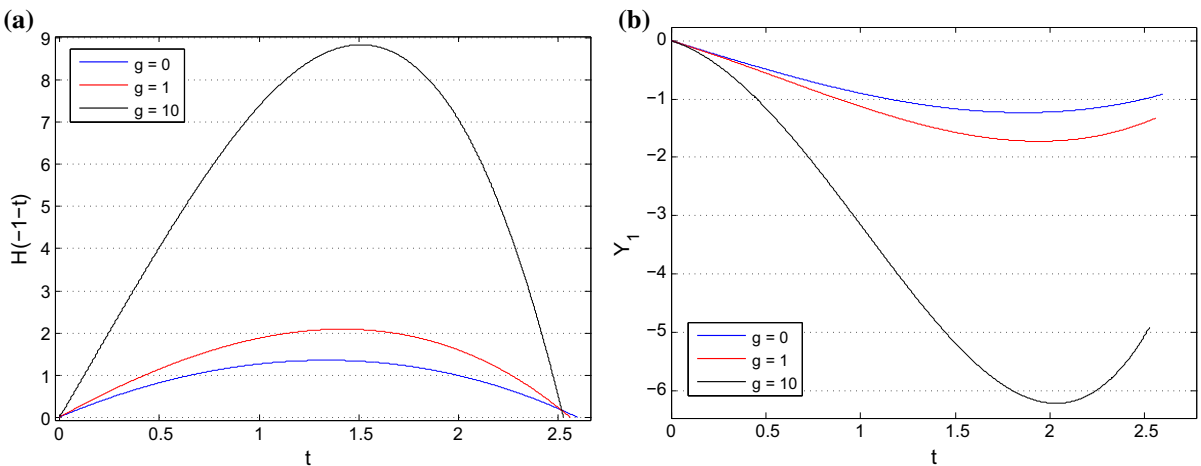


Fig. 6 Solutions of the linearised flooding system for $h(-1-t)$ and Y_1 for varying values of gravity parameter \bar{A} . The initial conditions for the system are set to $\theta_1(0) = 0$, $\omega_1(0) = 0$ and $V_1(0) = -1$. **a** $\mathcal{H}(-1-t)$. **b** Y_1

the trailing edge. A time-marching finite-difference scheme is presented here, which for any given time step first solves the flux condition and the flow in region 1, then solves the flow in region 2 and iterates these two steps until the Kutta condition at the trailing edge is satisfied. We then present our numerical findings as well as analyse the circumstances under which the thin body is able to skim or sink under various flooding conditions.

4.1 A finite-difference scheme

It is useful to rearrange the governing equations into a format more suitable for numerical discretization. We begin by re-writing the flux condition (25f) as a boundary condition for H_1 at the leading edge:

$$H_1(-1, t) = \frac{1}{u_1(-1, t)} [1 - u_2(-1, t)H_2(-1, t)]. \quad (45)$$

The Bernoulli equation (24d) for region 1 has the following leading edge boundary condition for u_1 :

$$u_1(-1, t) = \sqrt{1 + 2\hat{g}[1 - H_1(-1, t) - H_2(-1, t)]}. \quad (46)$$

In region 2 we spatially integrate Eq. (25a) from the leading edge to a given point on the body such that

$$u_2(x, t) = \frac{1}{H_2(x, t)} \left[C_u - (x + 1)V - \frac{1}{2}(x^2 - 1)\omega \right], \quad (x \in [-1, 1]) \quad (47)$$

with C_u being a variable that captures the leading-edge boundary conditions of region 2:

$$C_u = u_2(-1, t)H_2(-1, t). \quad (48)$$

Likewise we can spatially integrate the fluid momentum equation (25b) from the leading edge to a given point on the body so that

$$\pi_2(x, t) = - \int_{-1}^x \frac{\partial u_2}{\partial t} ds - \frac{1}{2}u_2^2 - \hat{g}(H_1 + H_2) + C_p \quad (x \in [-1, 1]) \quad (49)$$

with C_p given as

$$C_p = \frac{1}{2}u_2^2(-1, t) + \pi_2(-1, t) + \hat{g}[H_1(-1, t) + H_2(-1, t)]. \quad (50)$$

Observe that Bernoulli's equation (25e) in region 2 is

$$\frac{1}{2}u_2^2(-1, t) + \pi_2(-1, t) + \hat{g}[H_1(-1, t) + H_2(-1, t)] = \hat{g} + \frac{1}{2}, \quad (51)$$

and therefore C_p can be expressed in the following equivalent form:

$$C_p = \hat{g} + \frac{1}{2}. \quad (52)$$

The dynamic pressure equation (49) can be applied at the trailing edge to obtain

$$\pi_2(1, t) = - \int_{-1}^1 \frac{\partial u_2}{\partial t} dx - \frac{1}{2} u_2^2(1, t) - \hat{g}[H_1(1, t) + H_2(1, t) - 1] + \frac{1}{2}. \tag{53}$$

The Kutta condition (25g) implies this dynamic pressure should be zero at this edge, hence

$$\int_{-1}^1 \frac{\partial u_2}{\partial t} dx + \frac{1}{2} u_2^2(1, t) + \hat{g}[H_1(1, t) + H_2(1, t) - 1] - \frac{1}{2} = 0. \tag{54}$$

The condition (54) is extremely useful for checking the consistency of our numerical solutions, particularly for u_2 over the grid of $x \in [-1, 1]$. We shall use this condition at each time iteration for solution accuracy checking.

The flooding system can now be discretized using a finite- difference scheme. To do so we introduce a time grid $t \in (0, T]$ and spatial grid $x \in [-1, 1]$; these two grids are discretized as $t = i \Delta t$ ($\Delta t = T/J, i = 1, 2, \dots J$) and $x = -1 + j \Delta x$ ($\Delta x = 2/K, j = 0, 1, 2, \dots K$). The boundary conditions (45) and (46) for u_1 and H_1 can be discretized, respectively, as

$$u1_0^i = \sqrt{1 + 2\hat{g}[1 - H1_0^{i-1} - H2_0^{i-1}]}, \tag{55a}$$

$$H1_0^i = (1 - u2_0^{i-1} H2_0^{i-1}) / u1_0^i. \tag{55b}$$

Here the subscript and superscript denote a variable’s spacial and time indexing, respectively.

The flow equations (24a) and (24b) in region 1 are discretized using an implicit forward Euler method as

$$\frac{u1_j^i - u1_j^{i-1}}{\Delta t} + u1_j^i \frac{u1_j^i - u1_{j-1}^i}{\Delta x} = -\hat{g} \left[\frac{H1_j^{i-1} - H1_{j-1}^{i-1}}{\Delta x} + \theta^{i-1} \right], \tag{56a}$$

$$\frac{H1_j^i - H1_j^{i-1}}{\Delta t} + \frac{u1_j^i H1_j^i - u1_{j-1}^i H1_{j-1}^i}{\Delta x} = 0. \tag{56b}$$

These two equations can be rearranged into the following forms for u_1, H_1 for $j \in [1, K]$:

$$u1_j^i = \frac{1}{2} \left[\sqrt{(u1_{j-1}^i + \frac{\Delta x}{\Delta t})^2 - 4\hat{g}(H1_j^{i-1} - H1_{j-1}^{i-1} + \Delta x \theta^{i-1})} + u1_{j-1}^i - \frac{\Delta x}{\Delta t} \right], \tag{57a}$$

$$H1_j^i = \frac{\Delta x}{\Delta x + \Delta t u1_j^i} \left(H1_j^{i-1} + \frac{\Delta t}{\Delta x} u1_{i-1}^i H1_{j-1}^i \right). \tag{57b}$$

For each time step i we solve the boundary conditions in (55), and then solve the flow equations (56) over the rest of the spatial grid for $j \in [1, K]$.

In region 2, the flow velocity and dynamic pressure equations (47) and (49) can be discretized via a forward Euler scheme as

$$u2_j^i = \frac{1}{H2_j^{i-1}} \left[C_u^i - j \Delta x V^{i-1} - \frac{1}{2} (j^2 \Delta x^2 - 2j \Delta x) \omega^{i-1} \right]; \tag{58a}$$

$$\pi_2^i = -\frac{\Delta x}{\Delta t} \sum_{k=0}^i (u2_k^i - u2_k^{i-1}) - \frac{1}{2} (u2_j^i)^2 - \hat{g}(H1_j^i + H2_j^{i-1} - 1) + \frac{1}{2}. \tag{58b}$$

The Kutta condition (54) at the trailing edge is discretized as

$$\frac{\Delta x}{\Delta t} \sum_{k=0}^N (u2_k^i - u2_k^{i-1}) + \frac{1}{2} (u2_N^i)^2 + \hat{g} (H1_N^i + H2_N^{i-1} - 1) - \frac{1}{2} = 0. \quad (59)$$

For a given time step i , once the flow equations of (58) are solved over the entire spatial grid ($x \in [-1, 1]$), we verify these solutions by checking the Kutta condition (59) is satisfied at the trailing edge.

The left-hand side of (59) can be viewed as a function of C_u^i , i.e.

$$\mathcal{F}(C_u^i) = \frac{\Delta x}{\Delta t} \sum_{k=0}^N (u2_k^i - u2_k^{i-1}) + \frac{1}{2} (u2_N^i)^2 + \hat{g} (H1_N^i + H2_N^{i-1} - 1) - \frac{1}{2}. \quad (60)$$

In order to find the root of $\mathcal{F}(C_u^i)$, we start with an initial estimate of $C_u^i = u2_0^{i-1} H2_0^{i-1}$, then use the Newton–Raphson method to iteratively find the accurate value of C_u^i and therefore $u2$. The accurate solution of $u2$ is in turn used to update the rest of the flow solutions in region 1 and 2 via an iteration cycle.

The vertical and angular momentum equations of the thin body in (26) are discretized as

$$Y_m^i = Y_m^{i-1} + \Delta t V^i, \quad (61a)$$

$$V_m^i = V_m^{i-1} + \frac{\Delta x \Delta t}{M} \left(\sum_{j=0}^K \pi 2_j^i - \frac{M \hat{A}}{\Delta x} \right), \quad (61b)$$

$$\theta^i = \theta^{i-1} + \Delta t \omega^i, \quad (61c)$$

$$\omega^i = \omega^{i-1} + \frac{\Delta x \Delta t}{I} \sum_{j=0}^K (j \Delta x - 1) \pi 2_j^i. \quad (61d)$$

Finally the depth of the region 2 H_2 can be solved as

$$H2_j^i = Y_m^i + (j \Delta x - 1) \omega^i \quad (i \in (0, J], j \in [0, K]). \quad (62)$$

The scaled body mass, moment of inertia and acceleration due to gravity, M , I and \hat{A} , respectively, are user-defined input parameters. It should be noted that even though in theory these parameters can be freely prescribed, their values have an impact on the global errors of the numerical scheme.

To see this we first observe that the vertical and angular momentum equations (61b) and (61d) have the terms $\Delta x \Delta t / M$ and $\Delta x \Delta t / I$ in their coefficients. Supposing the values of M and I are extremely small such that $\Delta x \Delta t / M > 1$ and $\Delta x \Delta t / I > 1$, then the rounding and local truncation errors in π_2 are magnified and grow with time, thus increasing the global errors of the solutions and rendering the numerical scheme possibly unstable. Therefore for small values of M and I , the grid's mesh sizes need to be sufficiently fine in order to prevent this “error magnification” effect, and consequently increase the computational demand of the numerical scheme. In a similar principle, if the buoyancy parameter \hat{A} is large such that the body's vertical acceleration in (61b) is essentially buoyancy driven, the numerical approximation errors in π_2 will have a smaller impact on the flooding system's overall solutions.

In the next section we shall analyse the behaviour of the flooding model via numerical solutions. In particular, we investigate the circumstances under which the solid body is either able to overcome the effects of flooding and achieve eventual lift off from water, or sinking deeper under water and the associated flow behaviour.

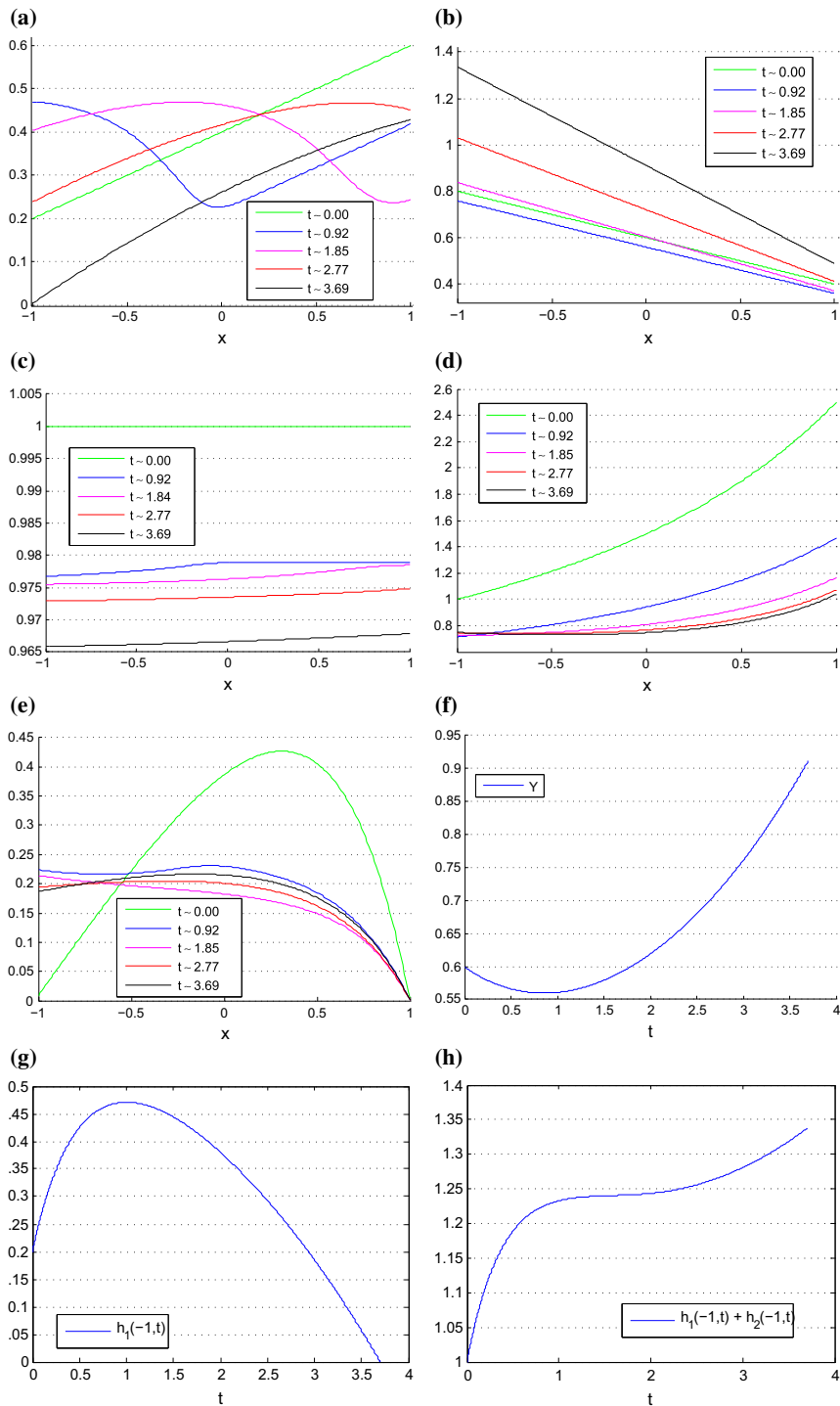


Fig. 7 A body re-emerging from under water over time. The body has scaled mass and moment of inertia of $M = 4, I = 1$, respectively, and is configured so that $Y_m(0) = 0.6, \theta(0) = -0.2, V_m(0) = -0.1$ and $\omega(0) = 0$. The scaled gravity and buoyancy terms are $\hat{g} = 0.1, \hat{A} = 0$. The body is initially completely submerged in water and has fresh flood coming over its body from the leading edge. At time $t \sim 3.69$, the leading edge of the body is able to rise above the incoming flood and re-emerge from water. **a** H_1 . **b** H_2 . **c** u_1 . **d** u_2 . **e** π_2 . **f** γ . **g** $H_1(-1, t)$. **h** $H_1(-1, t) + H_2(-1, t)$

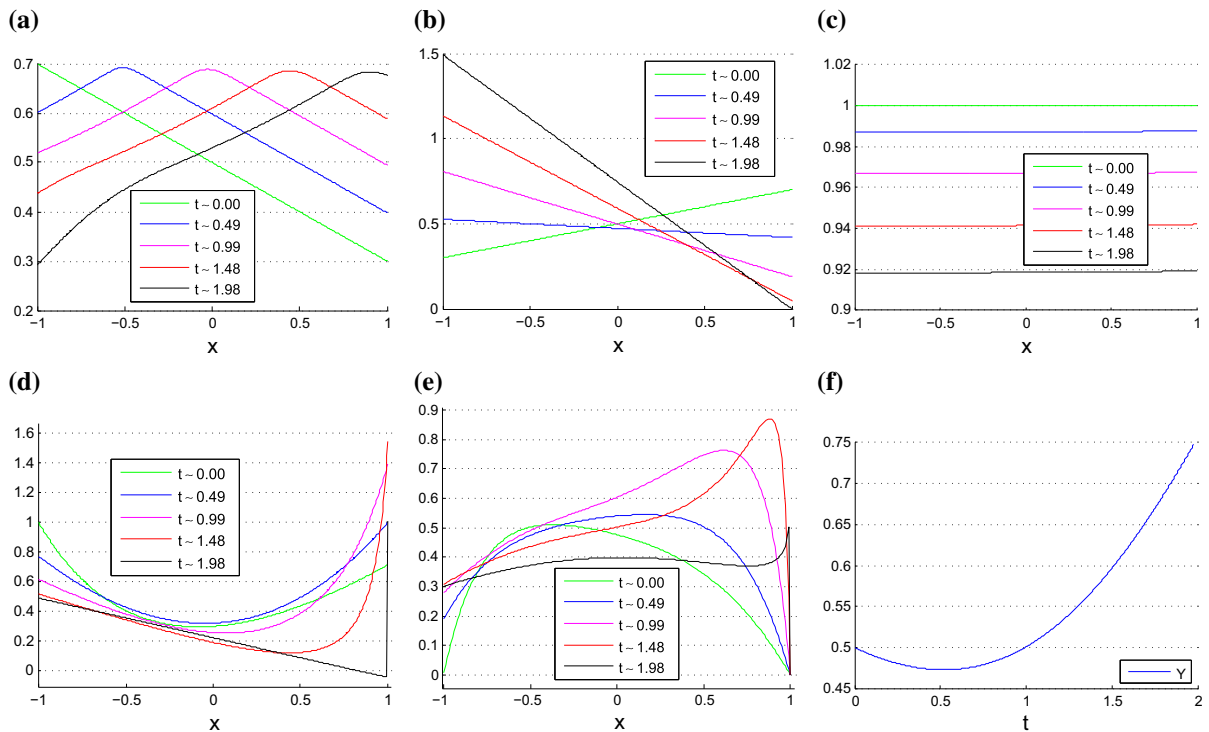


Fig. 8 Complete sinking: a flooded body whose trailing edge impacts upon the flow bed (asymptotically). The body has scaled mass and moment of inertia of $M = 4$, $I = 1$, respectively, and is configured so that $Y_m(0) = 0.5$, $\theta(0) = -0.2$, $V_m(0) = -0.1$ and $\omega(0) = -0.5$. The scaled gravity and buoyancy terms are $\hat{g} = 0.1$, $\hat{A} = 0$. The body is initially completely submerged in water. As the trailing edge of the body gets close to the flow bed, at $t \sim 1.98$ for instance, singularities in the flow speed u_2 and pressure π_2 begin to develop at this edge. **a** H_1 . **b** H_2 . **c** u_1 . **d** u_2 . **e** π_2 . **f** Y_m

4.2 Results

For an originally skimming body subject to flooding from its leading edge, depending on the flooding conditions as well as the body's physical characteristics such as buoyancy, the flooding model (24)–(26) yields two distinct outcomes: the body is either able to withstand the effects of flooding, go through a transition phase fully or partially under water and eventually emerge from the water again; or it is unable to obtain sufficient lift from the ambient flow and sinks further into water until eventually hitting the solid flow bed. See Figs. 7, 8, 9, 10, 11 and 12. As part of our analysis, we shall investigate the conditions under which such two distinct outcomes may be produced, as well as the effects of gravity and body buoyancy in our flooding model.

4.3 Complete sinking or re-emergence

For the purpose of the current numerical study, the sinking of a body is characterised by the water depth H_2 decreasing close to zero under a section of the body. For a thin flat body with non-zero contact angle this can be at either its leading or trailing edge, and as we shall see such a phenomenon is associated with singularities in the solutions of flow velocity and hydrodynamic pressure u_2 and π_2 in finite time. Hence when the body becomes sufficiently close to the flow bed it produces an extreme ground effect, whereby the flow speed and pressure in a surrounding region become extremely large. At such time our numerical scheme breaks down and a new flooding model taking account of boundary layer and other possible effects will need to be developed.

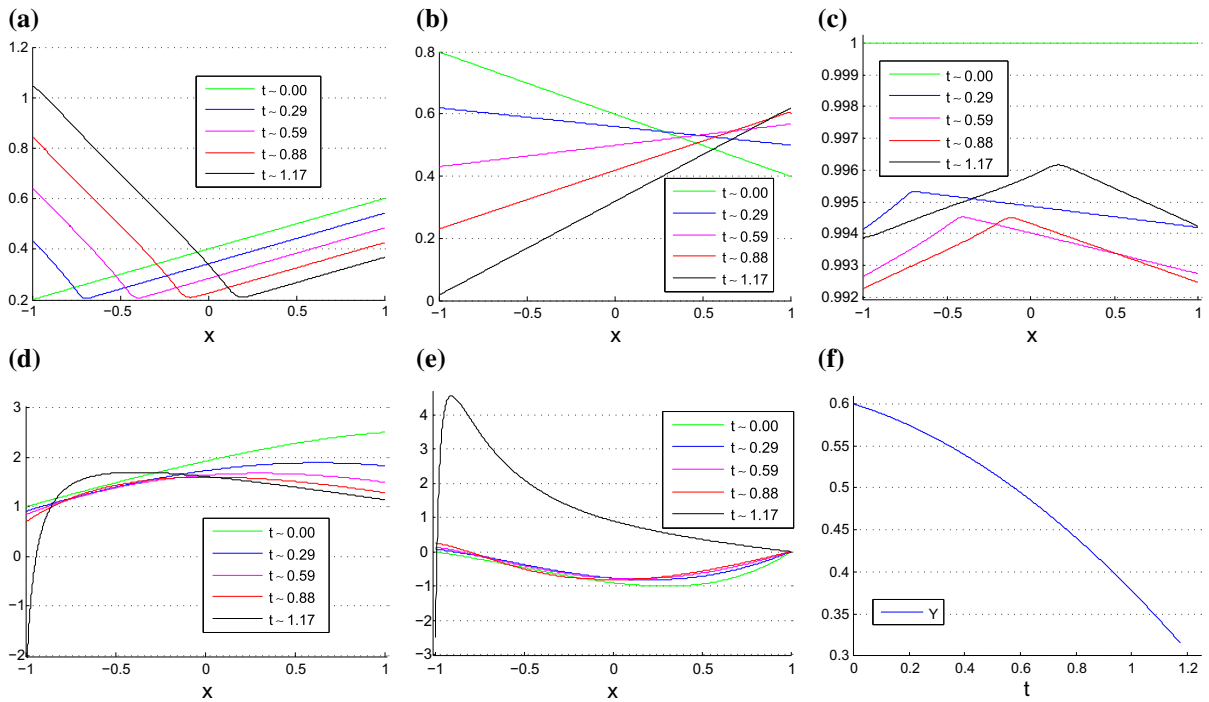


Fig. 9 Complete sinking: the leading edge of the flooded body impacts upon the flow bed. The body has scaled mass and moment of inertia of $M = 4$, $I = 1$, respectively, and is configured so that $Y_m(0) = 0.6$, $\theta(0) = -0.2$, $V_m(0) = -0.1$ and $\omega(0) = 0.5$. The scaled gravity and buoyancy terms are $\hat{g} = 0.1$, $\hat{A} = 0$. The body is initially completely submerged in water. As the leading edge of the body comes close to the flow bed, at $t \sim 1.17$ for instance, singularities in the flow speed u_2 and pressure π_2 begin to develop at this edge. **a** H_1 . **b** H_2 . **c** u_1 . **d** u_2 . **e** π_2 . **f** Y_m

The re-emergence of the body from underneath the flood, on the other hand, is signified by its leading edge rising above the free surface of the incoming displaced stream. In the numerical solutions this phenomenon is captured by the water depth variable $H_1(-1, t)$ at the leading edge decreasing to zero. From that point the body ceases to be flooded over by the incoming stream, and any residual water above the body will eventually exit into the downstream flow via the trailing edge. As soon as the upper surface of the body becomes dry the body resumes a skimming motion which is extensively discussed in [1, 3]. Note that if the scaled acceleration due to gravity $\hat{g} = \epsilon / Fr$ is small, then any hydrostatic effect of the flow above the flooded body can be neglected in our model (24)–(26), i.e. we can apply the atmospheric pressure condition at the upper surface of the body as soon as the flooding over the leading edge stops. In such a case the body effectively transitions into a skimming motion as soon as the flooding over the leading edge stops before its upper surface is completely dry.

For the purpose of computational simplicity we stop our numerical scheme as soon as $H_1(-1, t)$ becomes zero or close to zero, even though we could carry on with the solution by modifying the flux condition at the leading edge to account for $H_1(-1, t) = u_1(-1, t) = 0$ and marching our solutions until the upper surface becomes completely dry.

Figure 7 shows the response for a body that makes an initial angle of $\theta = -0.2$ with the flow bed and has an initial downward velocity of $V_m = -0.1$. This body is initially completely submerged in undisturbed water with free-surface height of one, i.e. $H_1(x, 0) + H_2(x, 0) = 1$, ($x \in [-1, 1]$). The solutions of the water depth H_1 at various times are given in Fig. 7a; note at the leading edge its depth at $t = 0$ has a positive value of 0.2. As time progresses this body first sinks deeper into water, but a short time after ($t \sim 0.99$) it begins a process to emerge from the water again. This can be seen in the solutions of the body’s vertical centre of mass position Y_m over time in Fig. 7d. The flooding over the body comes to a stop at $t \sim 3.7$, at which point the leading edge of the body rises to the same height as the incoming displaced stream, which is signified by the water depth H_1 decreasing to zero

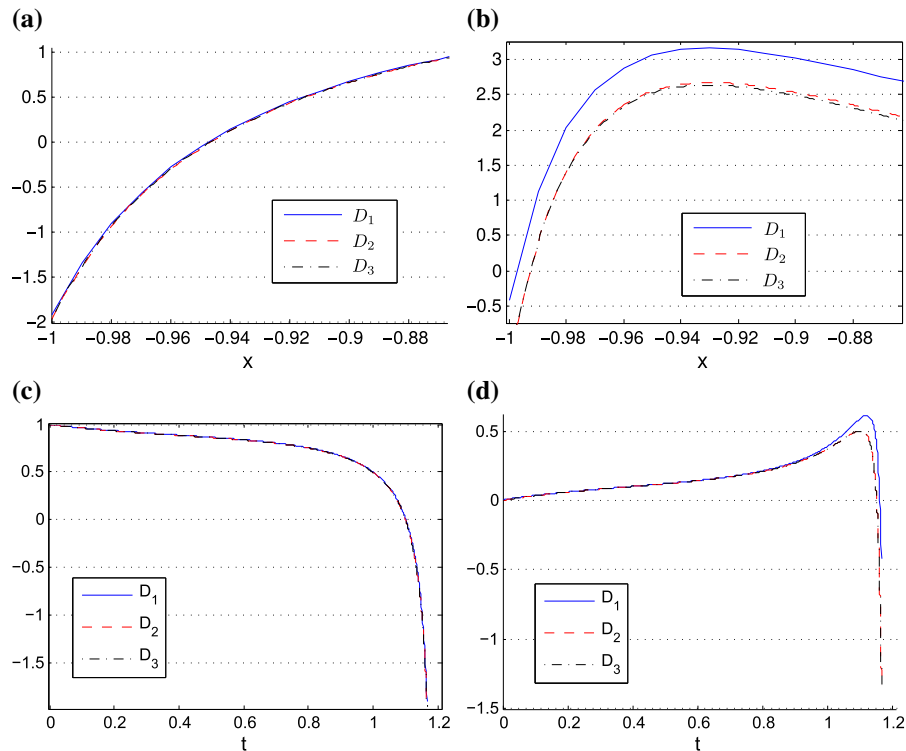


Fig. 10 Numerical solutions of u_2, π_2 in the flow region under the body for various grid step sizes. The initial conditions are the same as those given in Fig. 9, and the solutions of u_2 and π_2 are sampled at $t = 1.17$, which corresponds to the leading edge touching down on the flow bed. The grid step sizes of $D_1 = (\Delta x, \Delta t)$ are set to $(10^{-2}, 10^{-3})$, and D_2, D_3 are set to $(10^{-3}, 10^{-4})$ and $(10^{-3}, 5 \times 10^{-5})$, respectively, **a** $u_2(x, 1.17)$. **b** $\pi_2(x, 1.17)$. **c** $u_2(-1, t)$. **d** $\pi_2(-1, t)$

at the leading edge as shown in Figs. 7a, e. Since the flood from the leading edge propagates above the body in the form of shallow water waves, at early times when part of the flow close to the trailing edge has not yet felt the effects of flooding, “sharp-corners” can be seen in the solutions of H_1, u_1 , (i.e. Fig. 7a, b at $t \sim 0.92$ and $t \sim 1.85$).

Figure 7g shows the depth of the water over the body at the leading edge over time, $H_1(-1, t)$. At early times ($t < \sim 0.99$) the body descends deeper into water while the flow depth above the body $H_1(-1, t)$ increases; as the body eventually begins to ascend ($t \geq \sim 0.99$) this depth $H_1(-1, t)$ decreases. Figure 7f shows the height of the free surface at the leading edge, i.e. $H_1(-1, t) + H_2(-1, t)$. Note this height increases from $t = 0$ to $t \sim 3.69$, the time at which the body’s leading edge re-emerges from water.

Figures 8 and 9 demonstrate cases where the body’s leading and trailing edges come close to hitting (impacting upon) the flow bed, respectively. Under such circumstances we witness an extreme ground effect where the hydrodynamic pressure in a surrounding region under the body becomes large, while the flow speed goes through rapid adjustments in such a region.

In the case of the body’s trailing edge moving close to the flow bed, the hydrodynamic pressure under the body increases rapidly in a region close to this edge. However, the Kutta condition demands the hydrodynamic pressure to be zero at the edge of flow separation. We therefore witness a rapid decrease of pressure near the trailing edge of the body, see Fig. 8e; corresponding to such a rapid pressure drop, Fig. 8d shows that the flow speed grows very close to this edge. The pressure and flow velocity gradients $\partial\pi_2/\partial x, \partial u_2/\partial x$ become almost discontinuous at this edge as the body moves sufficiently close to the flow bed and our numerical algorithm is terminated. (This non-linear impact within finite time is consistent with the linearised findings of Sect. 3).

On the other hand when the leading edge of the body comes close to hitting the flow bed, a strong adverse pressure gradient develops in region 2 at the leading edge and in a small region after, and the hydrodynamic pressure grows

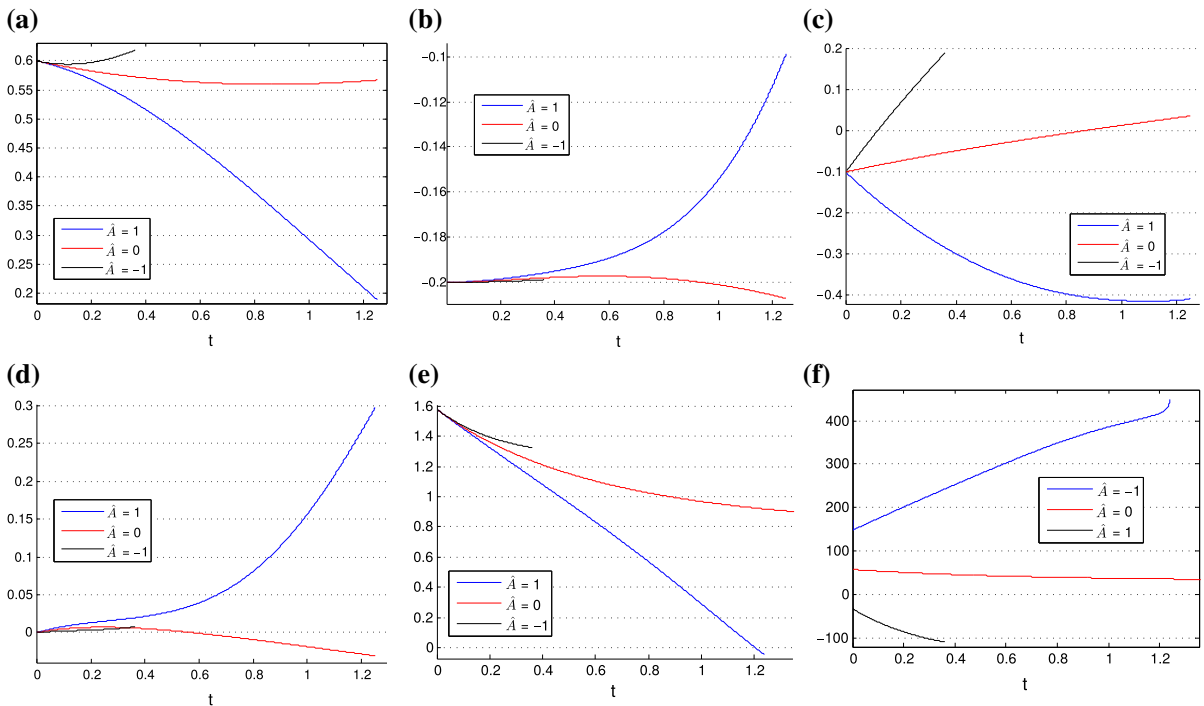


Fig. 11 Solutions of the flooding system with various values of the body buoyancy parameter \hat{A} . The body has scaled mass and moment of inertia of $M = 4$, $I = 1$, respectively, and is configured so that $Y_m(0) = 0.6$, $\theta(0) = -0.2$, $V_m(0) = -0.1$ and $\omega(0) = 0$. The scaled gravity term is $\hat{g} = 0.1$. The body is initially completely submerged in water and has fresh flood coming over its body from the leading edge. **a** $Y_m(t)$. **b** $\theta(t)$. **c** $V(t)$. **d** $\omega(t)$. **e** Average u_2 over time. **f** $\int_{-1}^1 \pi_2(s, t) ds$ over time

extremely large close to this edge, see Fig. 9e. This high pressure phenomenon is also accompanied by a reversed flow in a small region enclosing the leading edge, see Fig. 9d. As the body gets closer to the flow bed and $H_2(-1, t) \rightarrow 0$, the flow speed at this edge becomes negative and unbounded as implied by the conservation relation (47). As with the case of the body’s trailing edge hitting the flow bed, the pressure and flow velocity gradients $\partial\pi_2/\partial x$, $\partial u_2/\partial x$ grow extremely large, and our numerical algorithm terminates before their solutions become singular.

Given such rapid change of flow velocity and dynamic pressure in a subregion of the under-body flow, we check the accuracy of our numerical algorithm by solving the flow problem shown in Fig. 9 over three increasingly fine grids. The first grid, denoted as D_1 , on which we perform our numerical procedures is set to $(\Delta x, \Delta t) = (10^{-2}, 10^{-3})$. Repeating the procedures on two finer grids D_2 and D_3 , which are set to $(10^{-3}, 10^{-4})$ and $(10^{-3}, 5 \times 10^{-5})$, respectively, yields further two sets of solutions. The solutions of u_2 and π_2 derived from these three grids are given in Fig. 10. The comparisons tend to demonstrate that the set of solutions is largely robust as the grid step sizes are refined gradually.

4.4 Effects of gravity and body buoyancy

In this section, we analyse the effects of the body buoyancy as well as gravity in the ambient flow on the body that is subject to flooding.

The scaled buoyancy parameter \hat{A} represents the body’s acceleration due to the net effects of buoyancy and gravity. Here $\hat{A} = 0$ represents the body’s buoyancy cancelling out its gravitational effect; $\hat{A} > 0$ represents gravity overcoming buoyancy and vice versa. Figure 11 shows solutions of the flooding system for the cases of $\hat{A} = \{-1, 0, 1\}$, and in all cases the body is initially submerged in water. A buoyant body is able to emerge from the

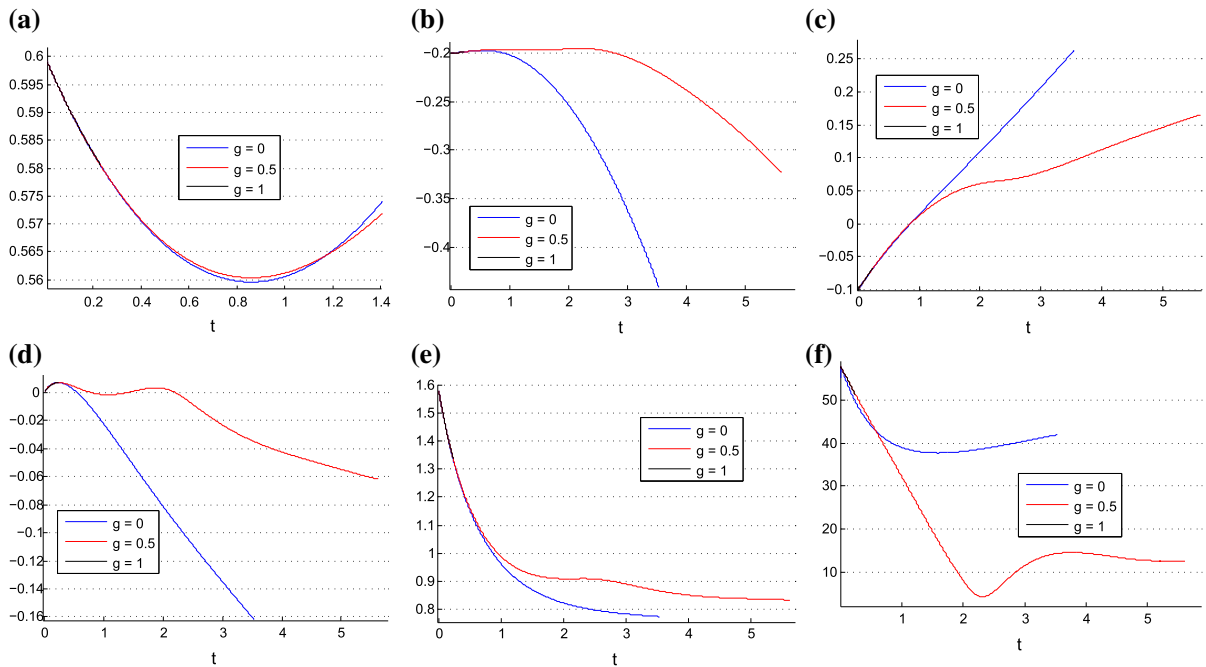


Fig. 12 Solutions of the flooding system with various values of the scaled gravity parameter \hat{g} . The body has scaled mass and moment of inertia of $M = 4$, $I = 1$ respectively, and is configured that $\hat{A} = 0$, $Y_m(0) = 0.6$, $\theta(0) = -0.2$, $V_m(0) = -0.1$ and $\omega(0) = 0$. The body is initially completely submerged in water and has fresh flood coming over its body from the leading edge. **a** $Y_m(t)$. **b** $\theta(t)$. **c** $V(t)$. **d** $\omega(t)$. **e** Average u_2 over time $\int_{-1}^1 \pi_2(s, t) ds$ over time **f** $\int_{-1}^1 \pi_2(s, t) ds$ over time

water rapidly as can be seen for the case of $\hat{A} = -1$, whose solutions terminate at $t \sim 0.3$ as its leading edge becomes dry. Note the net pressure force under the body is negative in this case (see Fig. 11f), i.e. there is a “suction” effect on the buoyant body as it rapidly emerges from water. The solutions for the case of $\hat{A} = 0$ have been given previously in Fig. 7, where the body is able to emerge eventually from water at $t \sim 3.69$ after a relatively longer underwater transition period. For the reduced-buoyancy case of $\hat{A} = 1$ where the body’s acceleration due to buoyancy is less than that of gravity, the body sinks rapidly towards the flow bed as can be seen in Fig. 11a, and at $t \sim 1.24$ the solutions break down. Note that the pressure force on the body, given by $\int_{-1}^1 \pi_2(s, t) ds$, becomes large as \hat{A} increases (see Fig. 11f), whereas the average flow speed in region 2 decreases more rapidly with increasing values of \hat{A} (see Fig. 11e).

To analyse the effects of gravity we prescribe our flooding system with three configurations of scaled gravity $\hat{g} = \{0, 0.5, 1\}$, where $\hat{g} = \epsilon / Fr$ with $\epsilon \ll 1$ and $Fr \sim O(1)$, $\hat{A} = 0$ for our given surfboard problem. Notice that the flux condition at the leading edge (46) in certain ways controls how large the scaled gravity can be—large values of \hat{g} force the solution of u_1 to become imaginary as the free-surface height at the leading edge becomes large, and specifically our flooding model fails when

$$H_1(-1, t) + H_2(-1, t) > 1 + \frac{1}{2\hat{g}}. \tag{63}$$

Figure 12 demonstrates the solutions for the three cases of scaled gravity. As the effects of gravity increase, the time required for the body to emerge from water also increases. This can be seen in Fig. 12a as the body’s leading edge emerges from water at $t \sim 3.7$ for $\hat{g} = 0$, whereas the required time for the case of $\hat{g} = 0.5$ increases to $t \sim 5.9$. For the case of $\hat{g} = 1$ our flooding system breaks down due to the solution of u_1 becoming imaginary in a very short time ($t \sim 0.2$). The hydrodynamic pressure force exerted on the lower section of the body decreases as the gravity effect increases as can be seen in Fig. 12f.

5 Conclusions

The main issue in this paper, on flooding of a body that is originally in a skimming motion, is whether the body sinks or erupts from the surrounding fluid (water) layer, a matter which has not been addressed previously as far as we know.

The water is assumed to be relatively shallow. The mechanisms active in deep water for a thin body which may either sink in or erupt out of the water could have an analogy or qualitative similarity to the mechanisms found in the present study for shallow water layers. For the latter, assuming the flow above and below the body detaches smoothly at the trailing edge, a localised pressure jump applies across the leading-edge station as if to satisfy the Kutta condition at the trailing edge. The 2D model also accommodates if necessary the buoyancy effect of the body, which in reality has an important role to play in the motions of a surfboard for example. Equally important for further study are 3D influences which for instance give flow around the sides of the body.

In the results, bounded instability is found first. A linearised analysis where the flow depth above the body is small in comparison to that underneath shows the original flooding model reduces to a system of linear equations. Under the pre-defined conditions the system has a finite positive eigenvalue, and perturbations eventually grow exponentially with time. Second, the complete non-linear flooding model allows investigation of various conditions under which a body is able to either emerge from the water or sink to the flow bed. The initial conditions play a key role. In particular when the body impacts upon the flow bed an extreme ground effect occurs, where the pressure becomes extremely large and reversed flow begins to develop. The finite-time touchdown analyses of [18,20] describe leading-edge or mid-chord impacts but it remains to be seen whether similar analysis applies to trailing-edge impact.

We further analysed the buoyancy and gravity effects on the flooding model. It is found that the less buoyant the body is, the greater the dynamic pressure force and the slower the flow speed under the body. Depending on how large the gravity effect is, the leading-edge flux and pressure jump conditions impose a limit on the free-surface height at this edge. The larger the effect of gravity, the smaller the leading-edge free-surface height the flooding model can sustain. The present work estimates the sink-times or eruption-times and their dependence on parameter values as in Figs. 7–12, the times being comparable with the characteristic ratio of body length divided by horizontal speed in general. In particular the analysis shows that a larger gravity effect decreases the hydrodynamic lift force on the body and therefore prolongs the time the body spends under water, a finding which is perhaps surprising. Finally here, this work gives the first self-consistent account of complete sinking as far as we know and likewise the first account of either submergence or part submergence followed by eruption of a body from the water. The question of which ending (sinking or eruption) occurs depends on the detailed flow and body parameters and also on the initial conditions of the fluid-body interaction involved throughout.

Acknowledgements We gratefully acknowledge the helpful comments and recommendations made by the referees.

Open Access This article is distributed under the terms of the Creative Commons Attribution 4.0 International License (<http://creativecommons.org/licenses/by/4.0/>), which permits unrestricted use, distribution, and reproduction in any medium, provided you give appropriate credit to the original author(s) and the source, provide a link to the Creative Commons license, and indicate if changes were made.

References

1. Hicks PD, Smith FT (2011) Skimming impacts and rebounds on shallow liquid layers. *Proc Roy Soc A* 467:653–674
2. Liu K (2017) Shallow water skimming, skipping and rebound problems. PhD thesis, UCL
3. Liu K, Smith FT (2014) Collisions, rebounds and skimming. *Philos Trans R Soc A* 372:20130351
4. Elliott JW, Smith FT (2017) Ice formation on a smooth or rough cold surface due to the impact of a supercooled water droplet. *Eng Math* 102(1):35–64
5. Hewitt IJ, Balmforth NJ, McElwaine JN (2011) Continual skipping on water. *J Fluid Mech* 669:328–353
6. Purvis R, Smith FT (2016) Improving aircraft safety in icing conditions. In: Aston PJ, Mulholland AJ, Tant KMM (eds) UK success stories in industrial mathematics. Springer, Berlin, pp 145–151
7. Tuck EO, Dixon A (1989) Surf skimmer planing hydrodynamics. *J Fluid Mech* 205:581–592
8. Sugimoto T (2003) Mechanics of the surf skimmer revisited. *Am J Phys* 71:144–149

9. Green AE (1935) The gliding of a plate on a stream of finite depth. *Proc Camb Philos Soc* 31:589–603
10. Green AE (1936) The gliding of a plate on a stream of finite depth. Part II. *Proc Camb Philos Soc* 32:67–85
11. Korobkin AA (1999) Shallow water impact problems. *J Eng Math* 35:233–250
12. Howison SD, Ockendon JR, Wilson SK (1991) Incompressible water-entry problems at small deadrise angles. *J Fluid Mech* 222:215–230
13. Korobkin AA, Ellis AS, Smith FT (2008) Trapping of air in impact between a body and shallow water. *J Fluid Mech* 611:365–394
14. Khabakhpasheva TI, Korobkin AA (2013) Oblique impact of a smooth body on a thin layer of inviscid liquid. *Proc R Soc A*.
15. Khabakhpasheva TI (2015) Impact of an elastic spherical shell on a thin fluid layer. *Fluid Dyn* 50(2):250–262
16. Reinhard M, Korobkin AA, Cooker MJ (2013) Water entry of a flat elastic plate at high horizontal speed. *J Fluid Mech* 724:123–153
17. Bowles RGA, Smith FT (2000) Lifting multi-blade flows with interaction. *J Fluid Mech* 415:203–226
18. Smith FT, Wilson PL (2011) Fluid-body interactions: clashing, skimming, bouncing. *Philos Trans R Soc A* 369:3007–3024
19. Kaur D (2013) Motion of a tethered blade beneath a free surface. Masters thesis, UCL
20. Smith FT, Ellis AS (2010) On interaction between falling bodies and the surrounding fluid. *Mathematika* 56(1):140–168
21. Smith FT, Wilson PL (2013) Body-rock or lift-off in flow. *J Fluid Mech* 735:91–119